Ocean Sci. J. (2015) 50(4):683–699
http://dx.doi.org/10.1007/s12601-015-0062-9

Article

Available online at http://link.springer.com

SpringerLink

Ocean Science Journal

pISSN 1738-5261
eISSN 2005-7172

The Simulation of a Storm Surge and Wave due to Typhoon Sarah using an Integrally Coupled Tide-surge-wave Model of the Yellow and East China Seas

Jin-Hee Yuk[1], Kyeong Ok Kim[2], and Byung Ho Choi[3]*

[1]*Disaster Management HPC Technology Research Center, Korea Institute of Science and Technology Information, Daejeon 34141, Korea*
[2]*Marine Radionuclide Research Center, KIOST, Ansan 15627, Korea*
[3]*Department of Civil and Environmental Engineering, Sungkyunkwan University, Suwon 16419, Korea*

Received 31 March 2015; Revised 29 July 2015; Accepted 13 August 2015

Abstract – The Yellow and East China Seas are characterized by shallow shelf seas, seasonal monsoons and typhoons, especially the Korean Peninsula's western coastal area, which features large tides, a complex coastline and many islands. This study implemented an integrally coupled tide-surge-wave model based on an unstructured grid to evaluate the impact of Typhoon Sarah, which occurred in September of 1959, on the Yellow and East China Seas and, specifically, the southern coast of Korea in terms of waves and storm surges. The model results projected a significant wave height of 2–7 m, a mean wave period of 4–14 sec, and positive surge heights that were 0.3–1 m along the southern coast of Korea. Additional model runs included two independent model runs for waves and tides, and one tide-surge model run was conducted to investigate the interactions in the wave, tide and storm surge processes. The coupled tide-surge-wave model reasonably reproduced wave properties and storm surges, but uncoupled models, i.e. independent models, slightly overestimated waves and surges. The wave forces associated with the gradient radiation stress resulted in water being elevated into coastal regions, thereby the water elevation increased onshore and the reverse happened offshore. A possible water level change due to a storm equivalent to Typhoon Sarah in the year 2100 was estimated by considering a mean sea level rise of 70 cm and was generally in the range of 70–100 cm in the Yellow and East China Seas and approximately 68 cm along the southern coast of Korea.

Key words – Coupled tide-surge-wave model, unstructured mesh, the Yellow and East China Sea, typhoon Sarah, tide-surge-wave simulation

1. Introduction

The recent introduction of unstructured wave models has made nesting unnecessary and the coupled system (unstructured-mesh SWAN and ADCIRC) can run on the same unstructured mesh. This identical and homogeneous mesh allows the physics of wave-circulation interactions to be correctly resolved in both models. The unstructured mesh can be applied to a large domain allowing all energy, from deep to shallow waters, to be seamlessly followed. There is no nesting or overlapping of structured wave meshes, and no interpolation is required. The problem of the wave reflection in the nesting boundary for the uncompleted feedback to the mother's domain did not need to be considered. The waves and storm surge were allowed to develop on the continental shelf and interact with the complex nearshore environment. The interactions in wave, tide and storm surge processes are noticeable within the shallow sea basin in cases of a severe storm. The Yellow and East China Seas are shallow shelf seas and feature large tides along the west coast of Korea, varying seasonally during monsoons and typhoons.

A previous study (Choi et al. 2003) developed a coupled tide-surge-wave model to investigate the effect of the interactions among tides, storm surges and wind waves due to Typhoon Sarah (5914), which occurred on September 14, 1959. The coupled model is based on the synchronous dynamic coupling of a third-generation wave model, WAM cycle 4, and a two-dimensional tide–surge model. Two additional model runs, i.e. the independent wave model run with meteorological wind fields and the wave model run with meteorological fields, sea surface elevations and depth-averaged current velocity fields from the tide-surge model in a loosely coupled manner, were performed and compared with the above coupled model regarding the coupling effect

*Corresponding author. E-mail: bhchoi.skku@gmail.com

on the Yellow and East China Seas.

This study also employed the coupled tide-surge-wave model, but this model was based on the unstructured grid (ADCIRC-SWAN). We computed the wave properties and storm surge due to Typhoon Sarah (5914) for the entire model domain, including the Yellow and East China Seas, and compared that with those computed by the above study (Choi et al. 2003). In addition, the interactions of waves and tide-surges were reviewed by comparing the coupled model results and independent model results.

The modeling procedures and results are presented and discussed in terms of the impact of Typhoon Sarah on the Yellow and East China Sea, especially the southern coast of Korea, which was greatly damaged, as well as the effect of the tide-surge-wave interaction and the applicability of the modeling system for hindcasting and forecasting a tide-surge-wave.

2. Typhoon Sarah (5914)

Typhoon Sarah occurred in September 1959, and intensified to a category 5-equivalent super typhoon on the Saffir–Simpson Hurricane Wind Scale (SSHWS). Typhoon Sarah peaked at 1-minute sustained winds of 310 km/h on September 15, and weakened to 185 km/h immediately before making landfall on southern Korea on September 17. The time when Typhoon Sarah made landfall on the southern coast of Korea was around Chuseok, which is one of the biggest national holidays in Korea, and, consequently, the extreme flooding and storm surge killed or left 849 people missing and injured 2,533 people, leaving approximately 370,000 victims. The flood washed away or destroyed 10,226 roads, 1,618 embankments, 152 plumb blocks and 2 bridges, and more than 9,000 ships were damaged or sunk. The property damage reached approximately $280 million (USD). Cumulatively, Typhoon Sarah was the worst natural disaster ever to befall Korea, especially the southeastern province of Korea, which was severely damaged, including a major city and the nation's largest port, Busan. During the period of Typhoon Sarah, a minimum barometric pressure of 951.5 hPa was observed at Busan on September 17, 1959, the highest level ever among the minimum pressure records in Korea.

Many areas in Japan were also directly affected by Typhoon Sarah. In the Ryukyu Islands of Japan, 6 people were killed, 6,000 homes were damaged and $2 million in crops were damaged due to the high winds and rain from Typhoon Sarah. The total for Japan was 99 dead and missing persons, and 509 injured individuals. The damage was severe in Okinawa and the Miyako Islands, where Typhoon Sarah was known as the '1959 Miyako-jima (Miyako-Island) Typhoon', because Japan Meteorological Agency (JMA) was responsible for naming the typhoon that struck Japan and caused great damage.

3. Numerical Model

Wave model

SWAN (Simulating WAves Nearshore) predicts in geographical space the evolution and time of the wave action density spectrum (N), with the relative frequency (σ) and wave direction (θ), as governed by the action balance equation (Booij et al. 1999):

$$\frac{\partial N}{\partial t} + \nabla_{\vec{x}}[(\vec{c}_g + \vec{U})N] + \frac{\partial c_\theta N}{\partial \theta} + \frac{\partial c_\sigma N}{\partial \sigma} = \frac{S_{tot}}{\sigma} \quad (1)$$

The terms on the left side of the equation represent, respectively, the change in the wave action in time, t, the propagation of wave action in space (where $\nabla_{\vec{x}}$ is the gradient operator in geographic space, $\vec{c}_g$ is the wave group velocity and $\vec{U}$ is the ambient current vector), the depth and current induced refraction and the approximate diffraction (with propagation velocity or turning rate c_θ), and the shifting of wave action due to variations in the mean current and depth (with propagation velocity or shifting rate c_σ). The source term, S_{tot}, represents the wave growth caused by wind; the action lost due to whitecapping, surf breaking and bottom friction; and the action exchanged between spectral components in deep and shallow water due to nonlinear effects. The associated SWAN parameterizations are provided by Booij et al. (1999), with all subsequent modifications as presented in version 40.72, including the phase-decoupled refraction–diffraction (Holthuijsen et al. 2003), although diffraction is not enabled in the present simulations. The unstructured-mesh version of SWAN implements an analog to the four-direction Gauss–Seidel iteration technique employed in the structured version, and it maintains SWAN's unconditional stability (Zijlema 2010). SWAN computes the wave action density spectrum at the vertices of an unstructured triangular mesh, and it orders the mesh vertices so it can sweep through them and update the action density using information from neighboring vertices.

Tide and surge model

ADCIRC (the ADvanced CIRCulation model) is a continuous-

Galerkin, finite-element, shallow-water model that solves for water levels and currents at a range of scales (Westerink et al. 2008; Luettich and Westerink 2004; Atkinson et al. 2004; Dawson et al. 2006). The details of this solution have been widely published (refer to http://www3.nd.edu/~adcirc/manual.htm for the User's Manual and Theory Report) and will not be stated here.

Coupling process

Figure 1 shows the schematic of the coupling of the tide-surge and wave model and the data communications between the two models. SWAN is driven by wind speeds, water levels and currents computed at the vertices by ADCIRC. Marine winds can be input to ADCIRC in a variety of formats, e.g. the format of wind velocity in x, y directions following an oceanographic convention (see User's Manual, http://adcirc.org/). ADCIRC spatially and temporally interpolates to project these winds to the computational vertices, and then it transfers them to SWAN. Information on water levels and ambient currents is calculated by ADCIRC and then is transferred to SWAN after recalculating the water depth and related wave processes, such as the wave propagation and depth-induced breaking. The ADCIRC model is partially driven by radiation stress gradients calculated using information from SWAN. These gradients, $\tau_{s,waves}$, are calculated as:

$$\tau_{sx,wave} = -\frac{\partial S_{xx}}{\partial x} - \frac{\partial S_{xy}}{\partial y} \quad (2)$$

$$\tau_{sy,wave} = -\frac{\partial S_{xy}}{\partial x} - \frac{\partial S_{yy}}{\partial y} \quad (3)$$

where S_{xx}, S_{xy} and S_{yy} are the wave radiation stresses (Longuet–Higgins and Stewart 1964; Battjes 1972).

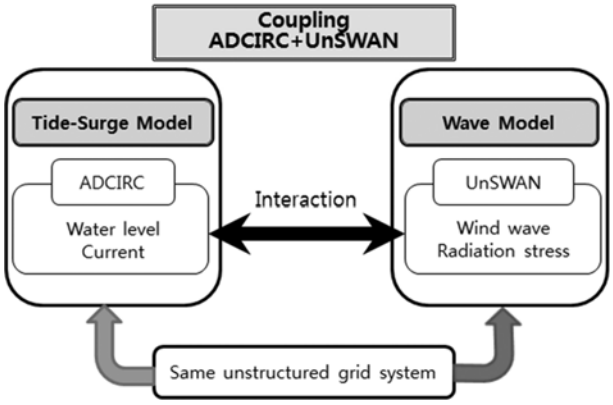

Fig. 1. Schematic of coupled ADCIRC and UnSWAN models and communications between two models

ADCIRC and SWAN run in series on the same local mesh and core. These two models leap frog through time, and each model is impelled by information from the other model (Dietrich et al. 2011). SWAN uses a sweeping method to update the wave information at the computational vertices. Thus, SWAN can take much larger time steps than ADCIRC, which has diffusion- and Courant-time step limitations due to its semi-explicit formulation and its wetting and drying algorithm. Consequently, the coupling interval is designed to be the same as the time step used for SWAN. As for the coupling between ADCIRC and SWAN, it is assumed that the waves are affected by circulation in the near-shore and the coastal floodplain; thus, ADCIRC runs first on the single coupling interval.

The coupling procedures between ADCIRC and SWAN are easily described by focusing on the single coupling interval. The single coupling interval is the same as the time step of SWAN stated above. At the beginning of a coupling interval, ADCIRC acquires the radiation stress gradients computed by SWAN at times corresponding to the beginning and end of the previous interval. ADCIRC uses that information by extrapolating the gradients of the previous coupling interval at all of its time steps in the current coupling interval. When the ADCIRC run is complete, the SWAN run is performed for one time step. At this time, SWAN takes the information from ADCIRC at the same time as ADCIRC. As described above, this information contains wind speeds, water levels and currents computed by ADCIRC at times corresponding to the beginning and end of the current coupling interval. These variables are averaged for the current one coupling interval, i.e. a single SWAN time step, and are used as forcing for SWAN at each time step. In short, ADCIRC uses the radiation stress gradients from SWAN, which is always extrapolated forward in time, whereas SWAN uses the wind speeds, water levels and currents from ADCIRC, which are always averaged to correspond with a single SWAN time step.

4. Model Setups

In this study, the mesh incorporated local resolution to approximately 300 m for the southern coast of Korea but also extended to the Yellow and East Seas and the western Pacific Ocean, including hundreds of islands, with a sufficient resolution for the wave-transformation zones near the coasts and an intricate representation of various natural and man-

made geographic features that collect and focus the storm surge in this region, amounting to 208,416 vertices and 383,715 triangular elements. The entire model domain used for all simulations is illustrated in Fig. 4.

To create the meteorological data field, we used Grid Point Values (GPVs) of the sea level pressure and air and sea surface temperatures with 6 hourly intervals and 50-km spatial intervals over the Northeast Asian seas as digitized by Japan Weather Association (JWA; https://www.jwa.or.jp). The GPVs dataset were interpolated to 1/12° grid resolution with a 1 hourly interval from a 6 hourly dataset for the model input. The wind fields to be imposed in the simulation were generated by embedding the strengthened typhoon's wind in the ambient wind field. The ambient marine wind fields in the entire model domain were computed by imposing a Planetary Marine Boundary Layer model (Cardone 1969). The strengthened typhoon's wind fields were computed using the Rankin vortex model (Fujita 1952) and then inserted into the ambient wind fields. Figure 2 shows the computed results of the pressure and wind vector fields for Typhoon Sarah (5914) at a 6-hr interval from 12:00 UTC on September 16. The computed maximum wind speeds in four moments from Fig. 2 ranged from 30 to 35 m/s. From the computed wind fields, the wind was approximately 20–30 m/s near the southern Korean coastline before and after the typhoon made landfall. The track of Typhoon Sarah (5914) is shown

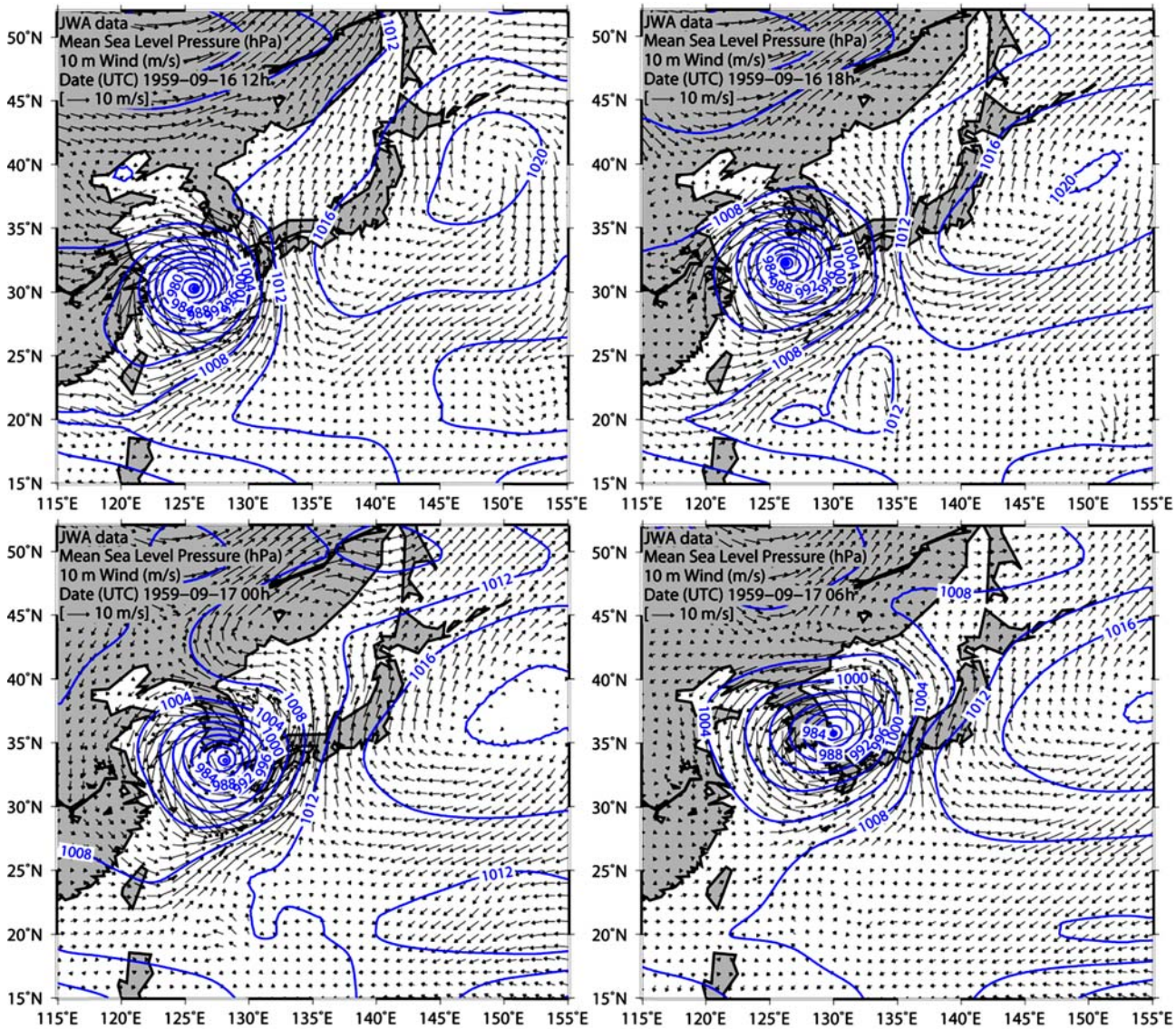

Fig. 2. Distribution of wind and pressure fields for Typhoon Sarah (5914)

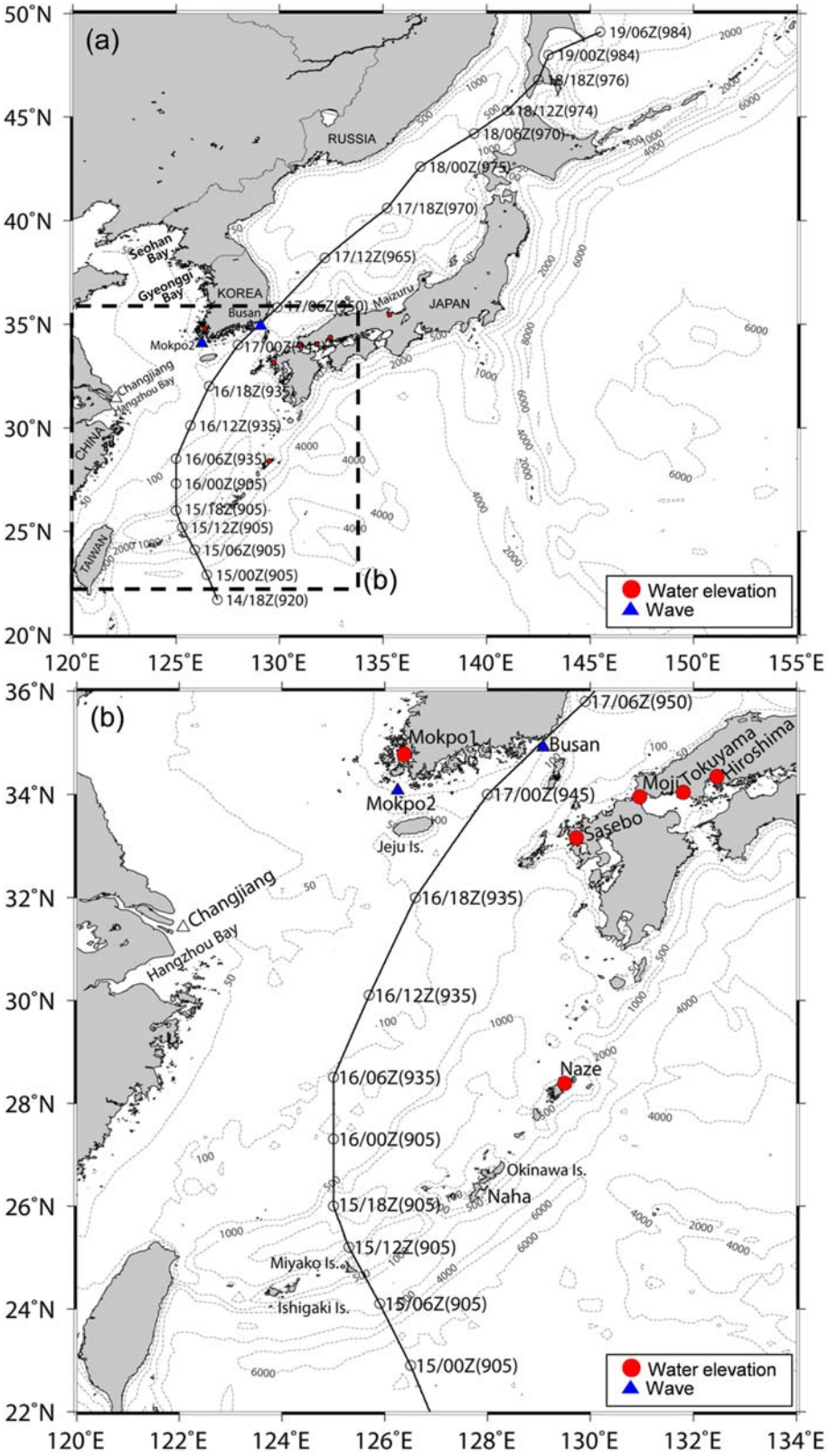

Fig. 3. Track of Typhoon Sarah (5914). The date format is day/hour in UTC and the numbers in the parenthesis indicates the typhoon center pressure (hPa). The gray dashed contours denote the water depth in meter. The bottom panel indicates the rectangular area surrounded with a thick and dashed line in the top panel

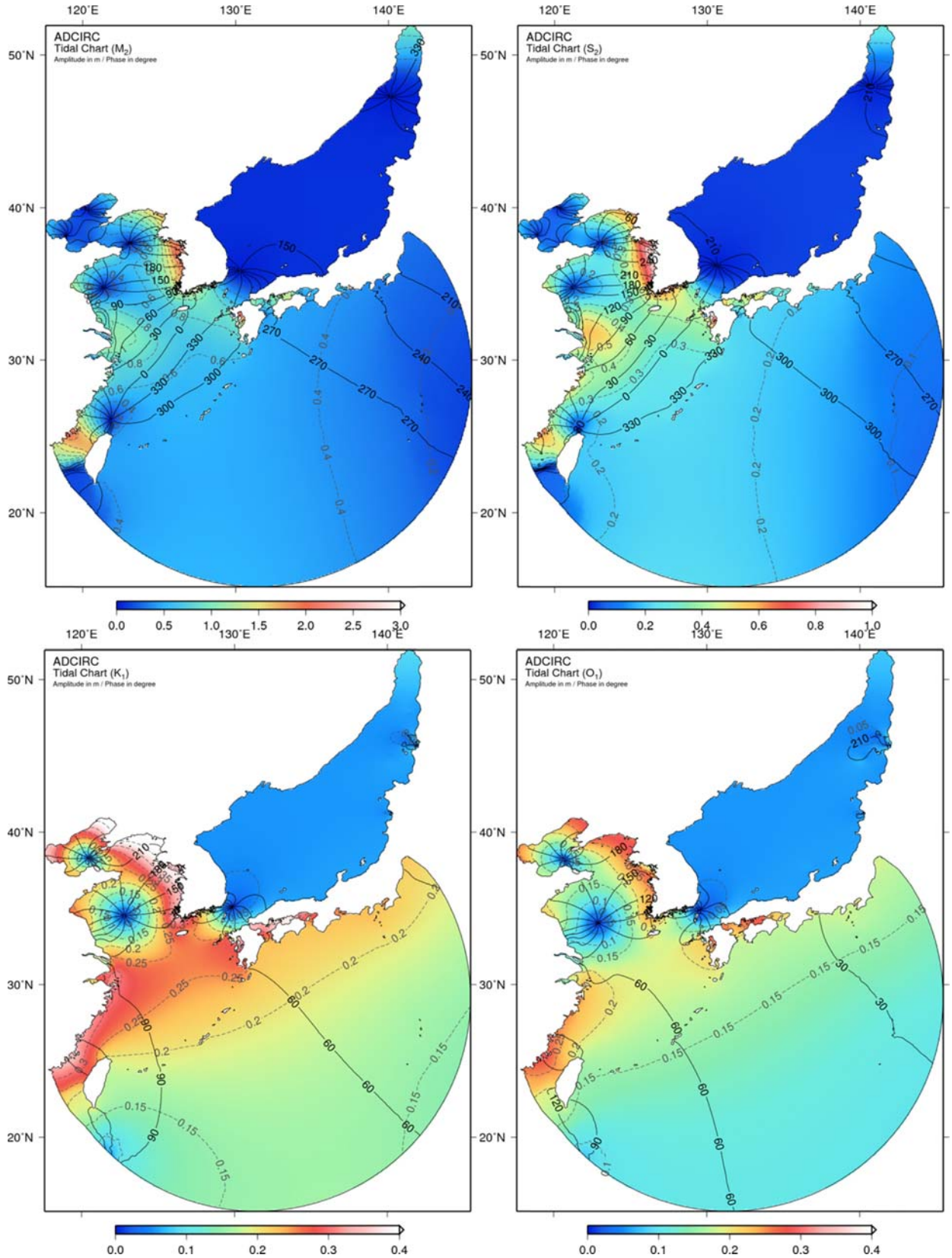

Fig. 4. Computed co-tidal charts of the M_2, S_2, K_1 and O_1 tides for modeled region. Dotted lines indicate the tidal amplitude (unit: m). Solid lines indicate the Greenwich phase (unit: degree) with interval of 30 degrees

in Fig. 3. Typhoon Sarah (5914) formed in September 1959 off the coast of Saipan and tracked northeastward with a pressure of 905 hPa and winds up to 65 m/s over northeastern Taiwan at a speed of approximately 25 km/h. It then moved north and northeastward with a pressure of 945 hPa, passing south of the Korean Peninsula. It continued to move northeastward, and dissipated on September 19 over northern Japan.

Open boundary forcing was applied in the form of the given specifications based on the National Astronomical Observatory (NAO) tidal predictions (Matsumoto et al. 2000) along the model's open water boundary. NAOTIDE is a program used to produce the ocean tidal prediction at a given time and location using an ocean tide model developed by assimilating TOPEX/POSEIDON altimeter data. Tidal elevations calculated based on the short-period and long-period tide-values at a specific location along the open water boundary and at the time-step over the model run time from the start to the end time epoch were imposed as the open boundary forcing. The major eight tidal constituents were calculated from the simulations of this study, and the four major tidal charts of M_2, S_2, K_1 and O_1 are displayed in Fig. 4. The tides were reasonably reproduced, which denoted that the tidal forcings with high accuracy were imposed in the simulations of this study.

The bottom friction coefficient was set to a variable value following the hybrid nonlinear bottom friction law among the options provided by ADCIRC. The friction coefficient was calculated from a quadratic bottom friction law in the deep water, whereas the friction coefficient increases with decreasing depth in shallow water.

For the coupling process between the ADCIRC and SWAN, the sea level pressures and wind field, which were predicted from JWA data, were imposed in ADCIRC. ADCIRC then transfers the wind speeds, water levels and currents, which were calculated at the vertices, to SWAN. The simulation in this study used the default settings, and the version of SWAN is 40.85. The ADCIRC time step is 0.5 sec. As previously described, the SWAN time step is equal to the coupling interval, which we set to be 300 sec. The total integration time is 4.75 days from September 14 18:00 UTC to September 19 12:00 UTC.

Three additional model runs were performed to investigate the effect of the wave-tide-surge interaction. These are the independent wave (W) model using only meteorological data, the independent tide (T) model using only tidal forcing on an open boundary, and the tide-surge (TS) model using the meteorological data and tides as forcings. Table 1 summarizes the numerical experiments with abbreviations.

Table 1. Experiment cases and their descriptions

Abbreviation of case	Description
T	Tide only
S	Surge by atmospheric forces
W	Wave only
TS	Surge by atmospheric forces and tide
TSW	Surge by atmospheric forces, tide and wave effects
TSW-T	Difference of TSW and T
TS-T	Difference of TS and T
TSW-W	Difference of TSW and W
TSW-TS	Difference of TSW and TS

5. Model Results

This integrally coupled tide-surge-wave model was also used for simulating Typhoon Maemi (0314) and Bolaven (1215) events and reproduced reasonable results (Choi et al. 2013; Kim et al. 2013). Validation of the Typhoon Sarah simulation was performed by comparing water elevations simulated from three models, i.e. TSW, TS and T models, and measured at tide gauges in Korea and Japan (Fig. 5). The measured tide data were obtained from Korea Hydrographic and Oceanographic Administration (KHOA; http://www.khoa.go.kr/) and Japan Coast Guard (JCG; http://www.jodc.go.jp/). The locations of the seven tide stations, one Korean and six Japanese, are depicted in Fig. 3. The simulation for Typhoon Sarah was not completely validated at many of the stations for the entire model domain because this typhoon event occurred in the distant past, in 1959; therefore, there were few observed data as shown in Fig. 3. Furthermore, the wave properties computed from this study were not validated because of the lack of wave data observed during Typhoon Sarah.

In general, the simulated water elevations showed good agreement with the observed data. Especially when there was little water disturbance due to the typhoon, the models reproduced good results, i.e. at the Naze, Tokuyama, and Hiroshima stations. Based on the differences in the water elevations calculated by the TSW (or TS) and T models, the maximum surge heights were found to be approximately 0.5–1.0 m at the Sasebo, Moji, Tokuyama and Hiroshima stations, which were near the intensified typhoon's track. The water displacements < 0.1 m were formed due to the

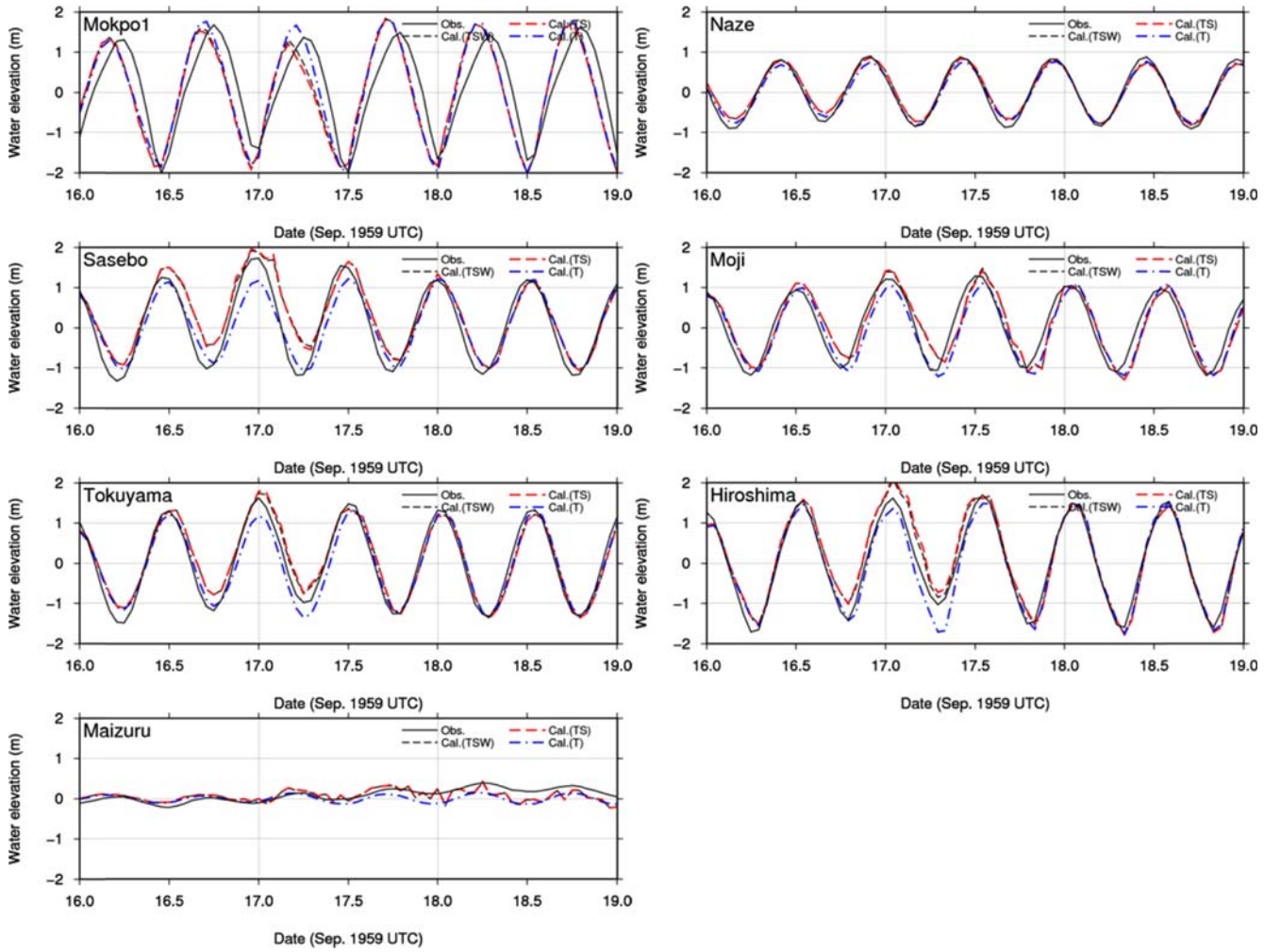

Fig. 5. Comparisons between observed and simulated water elevations. The three water elevations were simulated from the coupled tide-surge-wave (TSW) model, tide-surge (TS) model and tide (T) model

wave effect at the Mokpo1, Sasebo and Hiroshima stations, when evaluating that effect from the comparison between the water elevations of TSW and TS throughout the seven stations. The disagreements between the simulations and the observations appear to be attributed to the poor quality of some observation data, insufficient model mesh resolution, the misapplication of the bottom friction coefficient and the effect of shallow water depths and somewhat poor meteorological forcing. Indeed, the mesh resolution covering the sea areas around Japan was much coarser relative to the meshes around the Korean Peninsula; nevertheless, reasonable results were obtained in this study.

For comparison with the model study (Choi et al. 2003), the validation of models and the evaluation of coupling effects, we extracted the time series of the wave and current parameters computed by the coupled TSW, TS, T and W models together with winds at the Mokpo2 and Busan stations during the typhoon event (Fig. 6).

The water, surge elevations and wave period calculated by this study tend to be slightly lower than the model study (Choi et al. 2003) based on a WAM cycle 4 and 2D (two-dimensional) tide-surge model. These disagreements with the previous study's results may be due to the differences of the models used and, thus, the accompanying parameters. However, roughly, the variations obtained in our study at two stations appear to be very similar to the earlier study.

The maximum surge elevation had a negative value of approximately 0.5 m at the Mokpo2 station at approximately 6:00 UTC on September 17, and a positive value of approximately 0.3 m at the Busan station at approximately 3:00 UTC on September 17. There were few differences in surge elevations between the two calculations – TSW minus

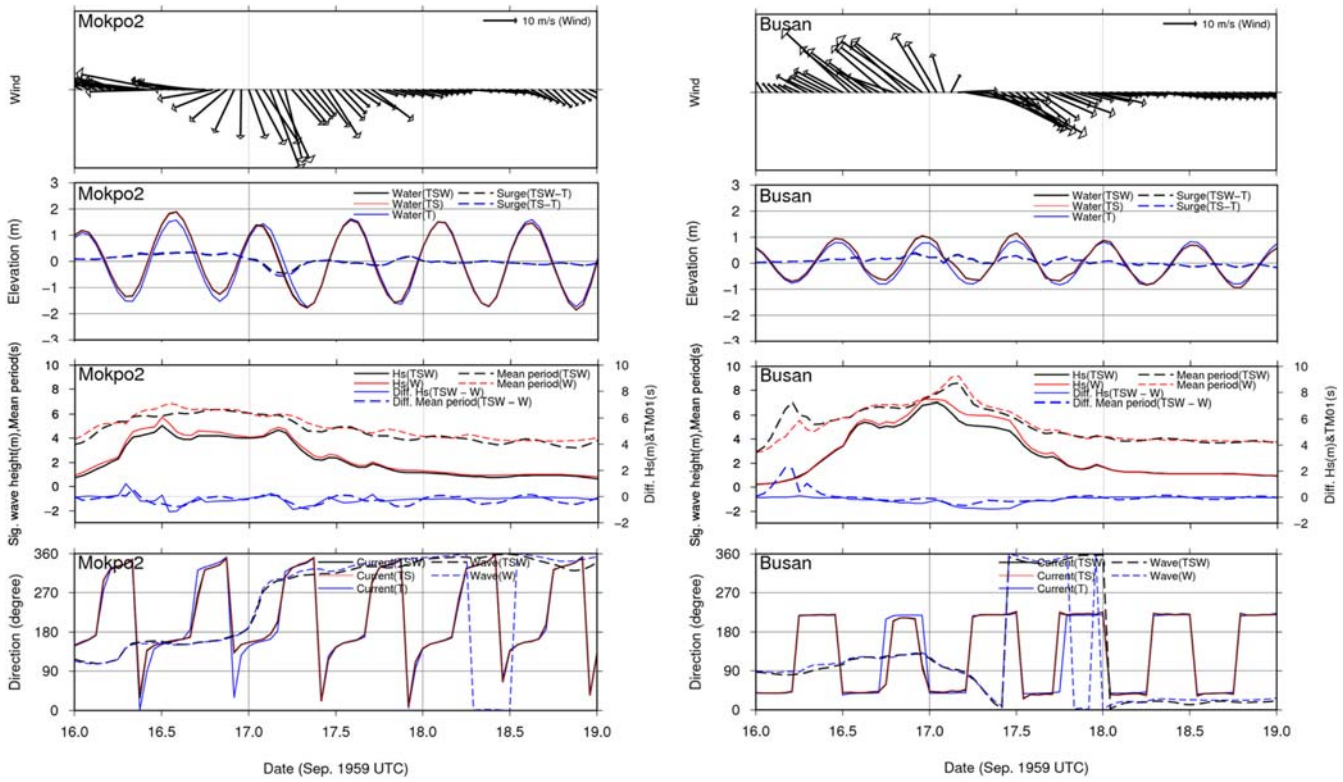

Fig. 6. Time-series of winds, water and surge elevations, significant wave heights, mean wave periods, mean wave directions and current directions at Mokpo2 and Busan stations. Abbreviations in legends indicate TSW: coupled tide-surge-wave model, TS: tide-surge model, T: independent tide model, W: independent wave model

T models and TS minus T models for both of the stations.

The time-series of the significant wave height and mean period denote that the TSW and W model results were similar at the two stations. The maximum significant wave height reached approximately 5 m at Mokpo2 and exceeded 7 m at the Busan station. Similar to the variation of the significant wave height, the maximum mean period was 7 and 9 sec at Mokpo2 and Busan, respectively. In general, the significant wave height and mean period computed by the TSW model were slightly lower than that computed by the W model at Mokpo2 and Busan during the typhoon event.

The wave height computed from the coupled model (TSW model) including the current-wave interaction was lower than that computed from the uncoupled model (W model) at the Mokpo2 and Busan stations. This tendency was also shown in earlier studies (Kim and Yamashita 2008; Ozer et al. 2000). According to Kim and Yamashita (2008), high wave conditions lead to high wave dissipation, and consequently generate a high water level elevation. This relation is applied in the case of the one-way effect from wave to current. High water level elevation causes the water to be deeper. Because the wave energy flux is conserved, the deepened water makes the wave height decrease according to the relationship $H^2\sqrt{d}$ = constant, where H is the wave height and d is the water depth. The reduced wave affects the current and the water elevation again. This cycle is generated in the case of a two-way wave-current interaction, i.e. it is applied to the coupled tide-surge and wave (TSW) model. Ozer et al. (2000) showed that a smaller total depth obtained from the coupled TSW model ultimately resulted in a significantly smaller wave height, namely the surge elevations associated with wave-dependent surface stresses only (the coupled TSW model) are generally smaller than those computed from a conventional run of the hydrodynamic model using the surface stress computed following Heaps (1965) and the bottom stress related with the wind stress. Therefore, the smaller total water depths induced more bottom dissipation and, thus, a significantly smaller wave height.

The time-series of the differences in the significant wave heights (H_s) and mean wave periods computed by both the TSW and W models are also illustrated with those of H_s and the mean period to investigate the effect of the coupling

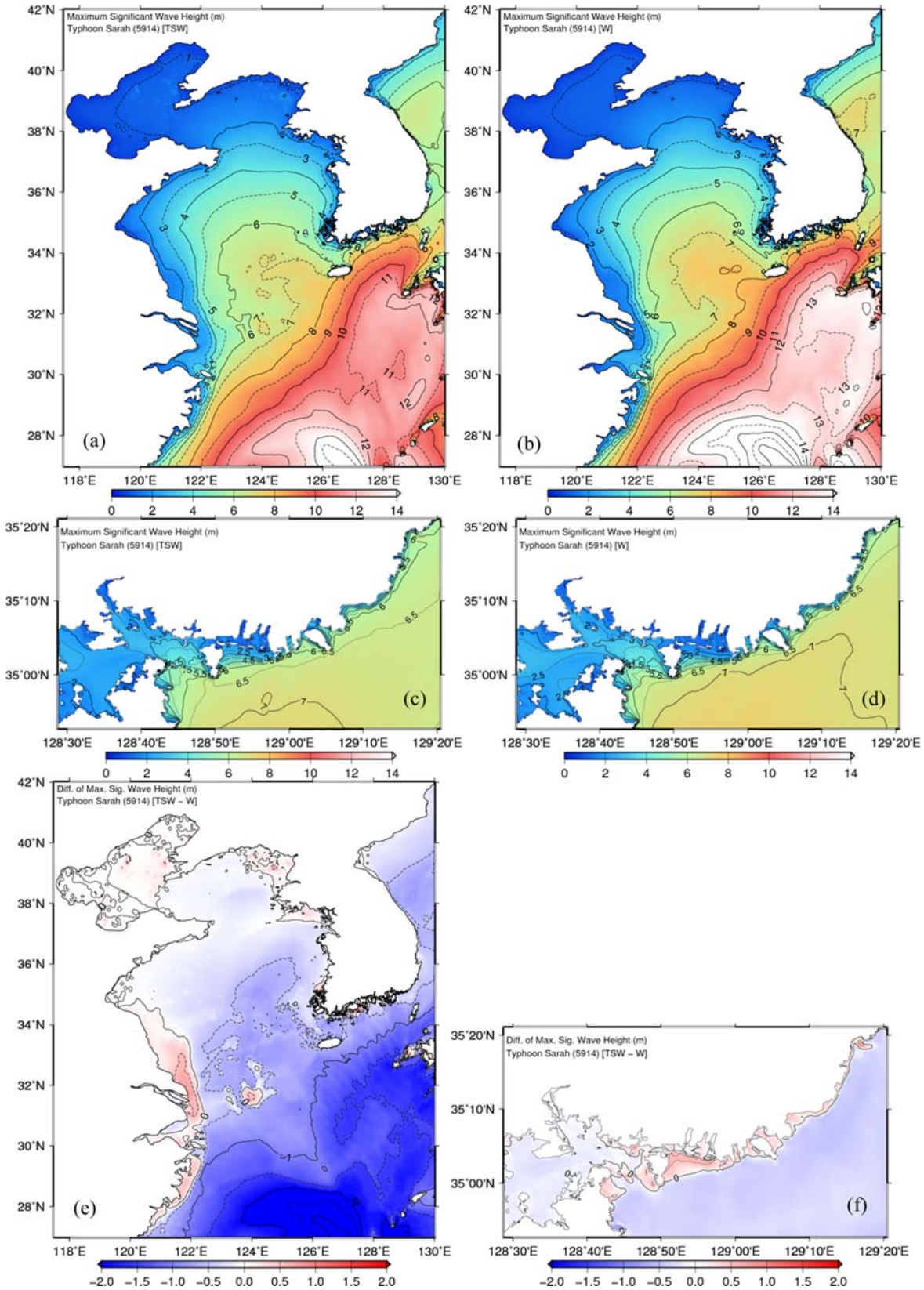

Fig. 7. Maximum significant wave heights for tide-surge-wave (TSW) and wave (W) models. The bottom figures indicate the difference between maximum significant wave heights of TSW and W models (between the above two cases)

processes on waves. The impacts of semi-diurnal tides on waves were distinguishable because the difference in the mean periods of the TSW and W models clearly exhibited wave modulation at the two stations.

The mean wave directions and current directions computed by the TSW, TS, T and W models are also shown in the bottom panels. The wave had been influenced while the typhoon was approaching the two stations (until approximately 12:00 UTC on 17 September). Thus, the former wave directions were different from the latter ones at the threshold of 6:00–12:00 UTC on 17 September at the two stations. Additionally, there were relatively different current directions of the TSW and TS models at the former time.

A previous study (Min 2011) employing the same coupled system as this study suggested that the coupled system reproduced the results more accurately than the uncoupled system. Therefore, we placed emphasis on the results from the coupled model (TSW model), compared them with the results from the uncoupled systems and accounted for the effect of the coupling processes. Accordingly, we presented the spatial distributions of the maxima of the TSW and the uncoupled models' results and the difference between both of their maxima, which were obtained by subtracting the uncoupled model's result from the TSW model's result (Figs. 7, 9 and 10).

Spatial distribution of the wave

Figure 7 shows the distribution of the maximum significant wave height simulated by the TSW and W model in the Yellow and East China Seas and the southern coast of Korea including Busan. The southern coast of Korea was severely damaged by this typhoon, thus we also presented the enlarged distribution for this area. The largest values were computed along the typhoon's path. The highest significant wave height was approximately 16 m near Naha, Japan, which was located where the typhoon had the lowest center pressure of 905 hPa.

The appearance of the wave (W) model contours was similar to the result of the coupled tide-surge-wave (TSW) model; but, in general, the value was larger than the TSW model result, except for the east coast of China (near Changjiang). We calculated the difference between the significant wave heights of the TSW and W models to quantify the effect of the tide-surge-wave interaction by subtracting the significant wave height of the W model from that of the TSW model. Figs. 7e–f denote the maximum differences of H_s between the TSW and W models. Positive differences were also found near the southern coast of Korea, but generally the wave (W) model overestimated the significant wave height. The difference between the two model results was the greatest (approximately -3 m) near Naha, Japan, and was approximately -1 m along the southern coast of Korea.

In previous studies (Min 2011; Choi et al. 2013), Typhoon Maemi (0314), the 14th in 2003, was simulated using the same coupled model as in this study. Typhoon Maemi was similar to Typhoon Sarah in terms of its track and strength and was the most powerful typhoon to hit the Korean Peninsula in a century. One of the hardest hit cities was Busan, which was also one of the cities damaged severely by Typhoon Sarah. Therefore, we presented the maximum significant wave height (H_s) due to Typhoon Maemi together with the H_s due to Typhoon Sarah for the southern coast of Korea, including Busan, from a perspective of disaster prevention and management (Fig. 8). The contours of the two distributions appear similar, each influenced by similar tracks of both of the typhoons, the complex coastlines and many islands, but the significant wave height due to Typhoon Maemi was approximately 1–7 m greater than the one attributed to Typhoon Sarah.

The maximum mean periods were calculated from two models and compared for the Yellow and East China Seas and the southern coast of Korea (Fig. 9). The mean periods were 5, 5 and 4–14 sec around the western coasts of Korea, near the mouth of Changjiang River, and the southern coast of Korea, respectively. In general, the wave period computed by the wave (W) model was longer than the coupled tide-surge-wave (TSW) model.

The phenomenon of the difference between the TSW and W models exists in terms of the significant wave height and the wave period over the Yellow and East China Seas as a result of the waves being modified by the bathymetry and coastline along the typhoon track.

Spatial distribution of the storm surge

Figure 10 depicts the distribution of the maximum positive surge height during Typhoon Sarah. The surge height was obtained by subtracting the maximum water elevation computed by the independent tide, the T model from the maximum water elevations computed from the tide-surge-wave, the TSW (or tide-surge, TS) model. The maximum water elevations computed from the tide-surge-wave (TSW) and tide-surge (TS) models during Typhoon Sarah exhibit a similar distribution. In Figure 10, 'TSW-T' indicates the water elevation computed

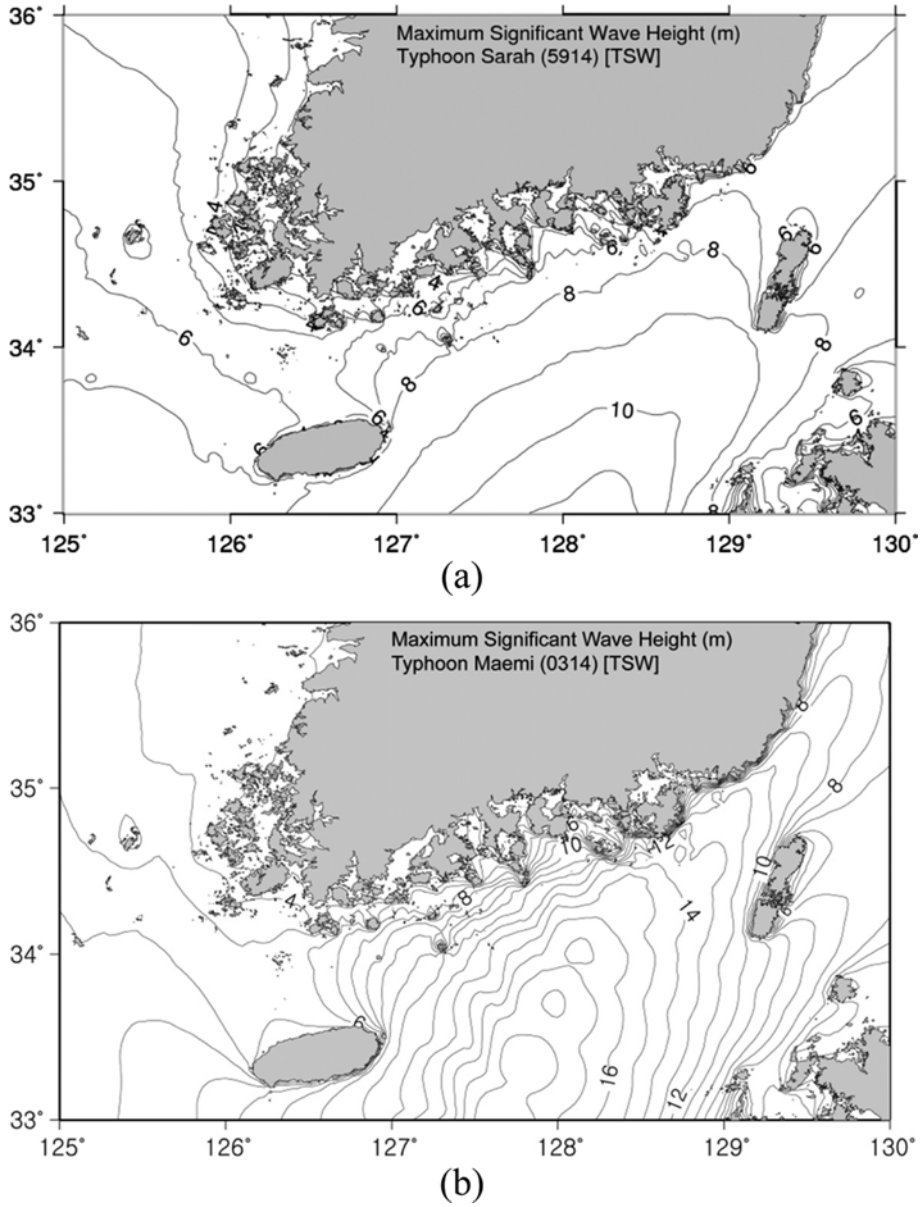

Fig. 8. Maximum significant wave heights computed by the coupled TSW model for (a) Typhoon Sarah (5914) and (b) Typhoon Maemi (0314)

from the tide-surge-wave (TSW) model minus the water elevation computed from the tide (T) model. The same process was applied in the case of 'TS-T'. The spatial distributions of the maximum positive surge heights from 'TSW-T' and 'TS-T' were similar. The largest positive surge height is located near the northwest region of the Changjiang River mouth, and the surge height exceeded 2 m. The surge height was approximately 0.3 m in the Yellow and East China Seas, and ranged from 0.3 to 1 m along the southern coast of Korea. The difference between the two surge heights computed above, indicating a difference in the maximum surge height field obtained from 'TSW-T' minus the maximum surge height field obtained from 'TS-T', is shown in Figs. 10e–f. In general, the maximum positive surge height computed from 'TSW-T (TSWT)' was slightly less than that computed from 'TS-T (TST)'. However, the contrary was shown in Hangzhou Bay and along the southern coast of Korea, which were affected by the wave.

Spatial distribution of the effect of radiation stress

We calculated the difference between the two water elevations obtained from the storm surge simulations with

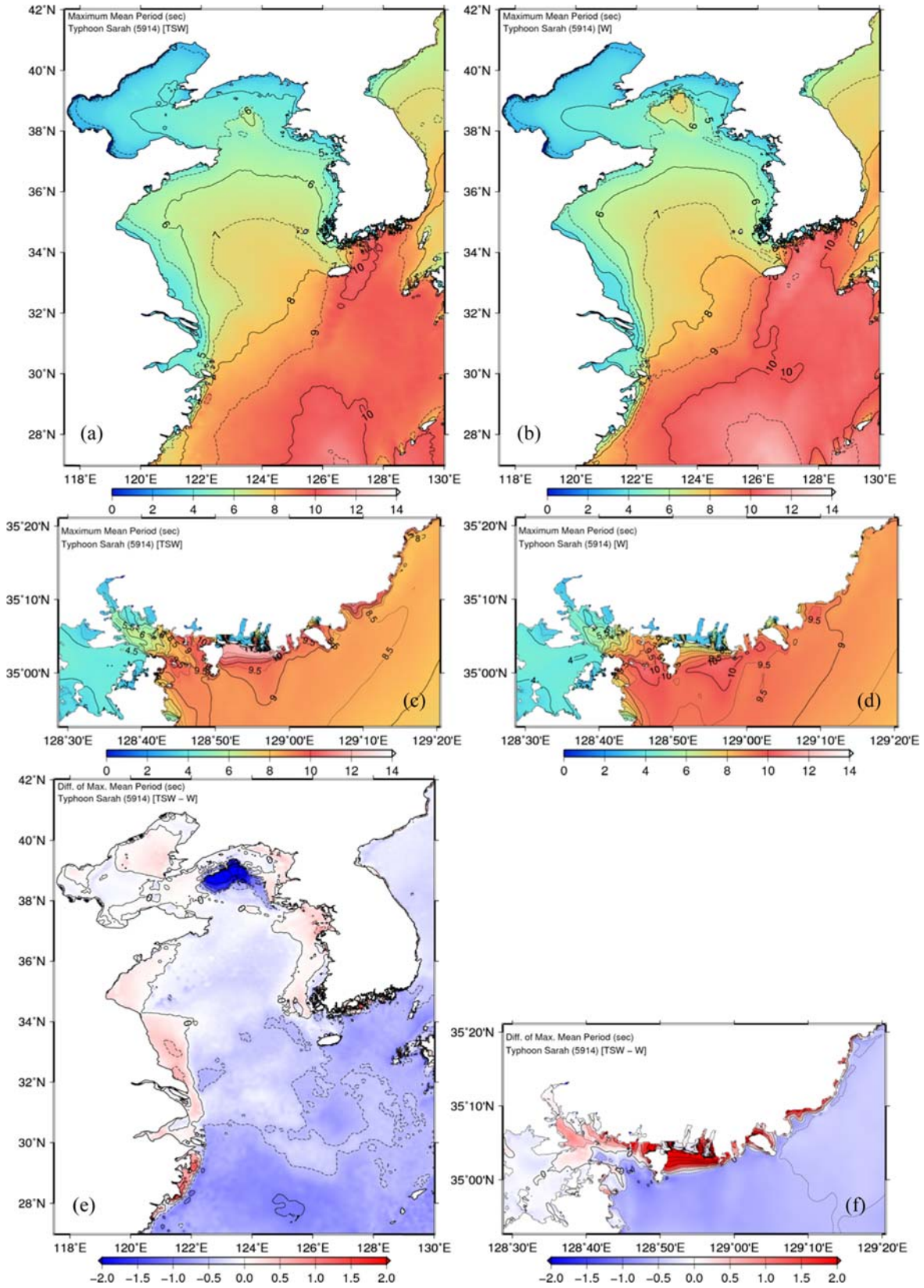

Fig. 9. Maximum mean wave periods for tide-surge-wave (TSW) and wave (W) models. The bottom figures indicate the difference between maximum mean wave periods of TSW and W models (between the above two cases)

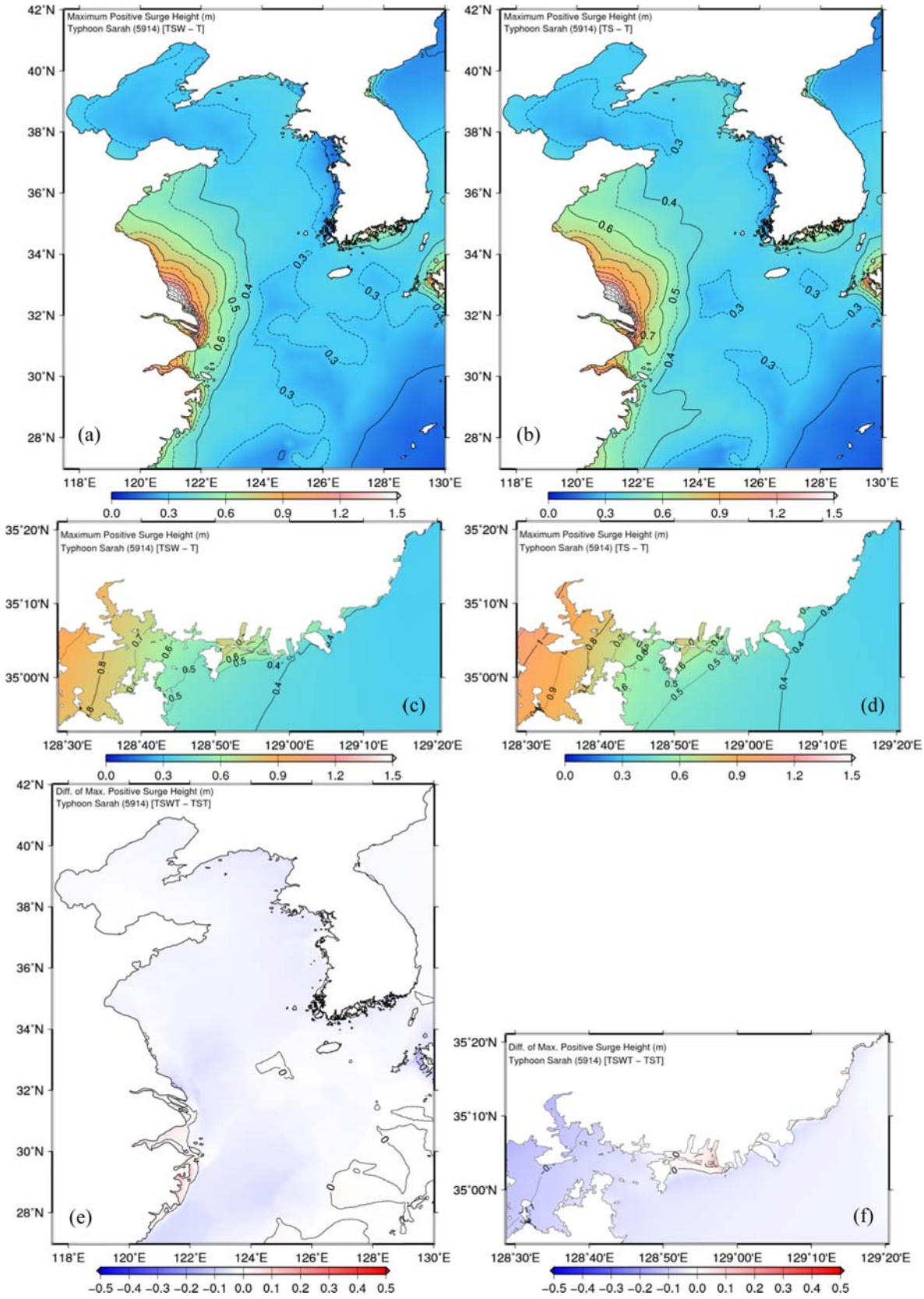

Fig. 10. Maximum positive surge heights computed from TSW minus T (TSW-T) and TS minus T (TS-T). The bottom figures indicate the difference between above two TSW-T and TS-T cases

waves and without waves, i.e. using the 'TSW' and 'TS' models to investigate the effect of waves, i.e. the water elevation change due to the gradient of radiation stress. A wave is not affected by the bottom topography in the deep sea, and it does not change the energy gradient. However, in the shallow waters that are influenced by the bottom topography, the gradient of radiation stress begins changing by a transition of the wave energy distribution due to dissipation and refraction (Choi et al. 2013).

Figure 11 plots the maximum differences between the two water elevations. In this figure, the positive values indicate where waves increased the water elevation; negative values indicate where waves decreased the water elevation. As a whole, the additional positive water elevation was due to waves that were computed in approximately all regions of the Yellow and East China Seas except the north and south regions of Hangzhou Bay and some regions along the southern coast of Korea. Generally, these local distributions of wave effects in the Yellow and East China Sea were similar to the differences in surge heights (Figs. 10e–f). This effect can also be seen in the difference in the maximum significant wave height and the mean period in Figs. 7 and 8, except for regions with very shallow waters north of the Changjiang River. The additional positive water elevation was approximately 0.1 m in the Yellow and East China Seas, and reached 0.2 m along the west coast of Korea. With regards to the southern coast of Korea (Fig. 11b), there was a setup (increase in water elevation) of 0.1–0.2 m along the southern coast of Korea, but a slight setdown (reduction in water elevation) offshore. The large fluctuations were simulated near the complex coastline and numerous islands because these served as barriers. The wave forces resulted in water being raised into the coastal region, thereby increasing the onshore water elevation. Conversely, the water elevation offshore decreased slightly. Similar to our results, the previous study (Choi et al. 2013) on the impact of Typhoon Maemi showed an increase in the sea elevation rise due to the gradient stress and its rate of 5–12% at shallow waters along the southern coast of Korea.

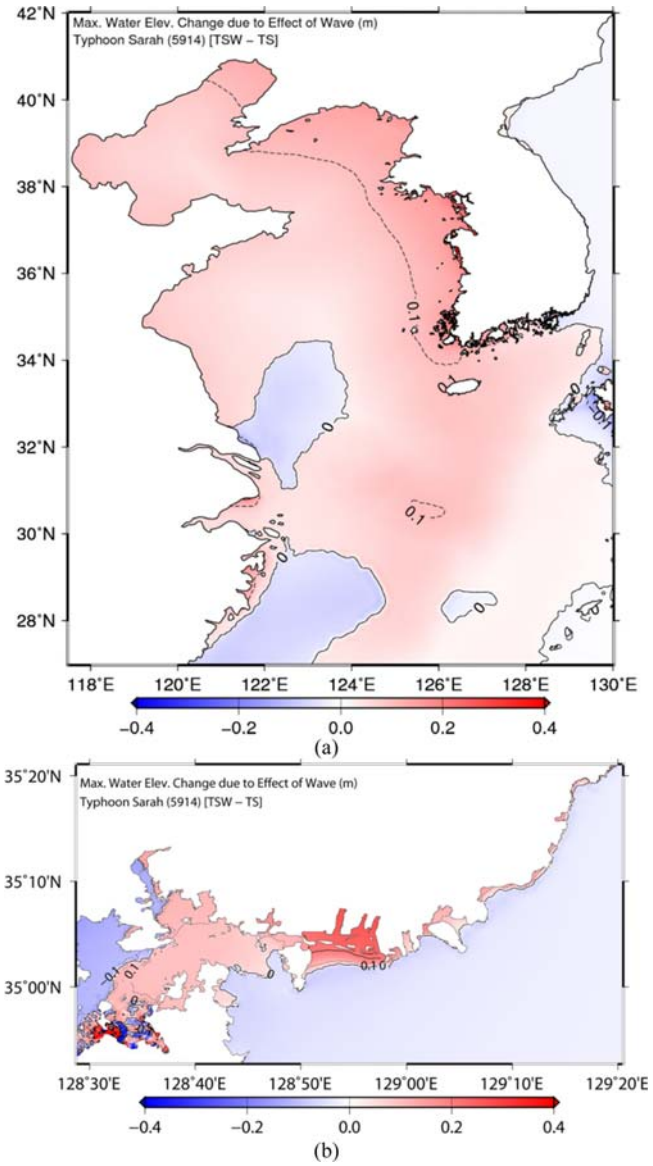

Fig. 11. Maximum difference of water elevations between the tide-surge-wave (TSW) and tide-surge (TS) models

6. Sea Level Prediction in the Year 2100 due to Typhoon Sarah

Temperature increase due to global warming is a major contributor to the intensification of typhoons; thus, a super typhoon is highly likely to occur in the future. For an adequate response to such an expected extreme condition, we investigated what Typhoon Sarah (5914) would be like if it occurred at the end of this century. The experiment was performed assuming the same meteorological input from an identical typhoon with the same tidal forcings, but the water depth was modified with the sea level rise. The water depth was uniformly increased by 70 cm across all the grids. The additional 70 cm is the projected mean sea level (MSL) change for the western and southern coast of Korea in the year 2100 compared to the level during the years 1980–1999 based on the Representative Concentration Pathways 4.5 (RCP4.5) scenario of the Intergovernmental Panel on Climate Change (IPCC)

fifth assessment report (KMA 2014). We then ran the coupled TSW model again with the same meteorological and tidal inputs but a modified MSL, resulting in different water depths. The difference in water depths affects the tide and surge dynamics, resulting in water levels that are different from those in the original model. The resulting difference between the maximum sea levels projected for 2100 and in 1959 is shown in Fig. 12. The increase in the MSL results in a largely increased water level in the Gyeonggi and Seohan Bays, with an increase in water levels of 80–100 cm and approximately 90 cm, respectively. Additionally, an increased water level of 70–80 cm was estimated along the coast of China. Contrary to the increase relative to the MSL rise (70 cm), a decrease in the relative MSL was observed along the southern coast of Korea, which was extensively damaged by Typhoon Sarah in 1959, and was quantified to be approximately 68 cm (Fig. 12b).

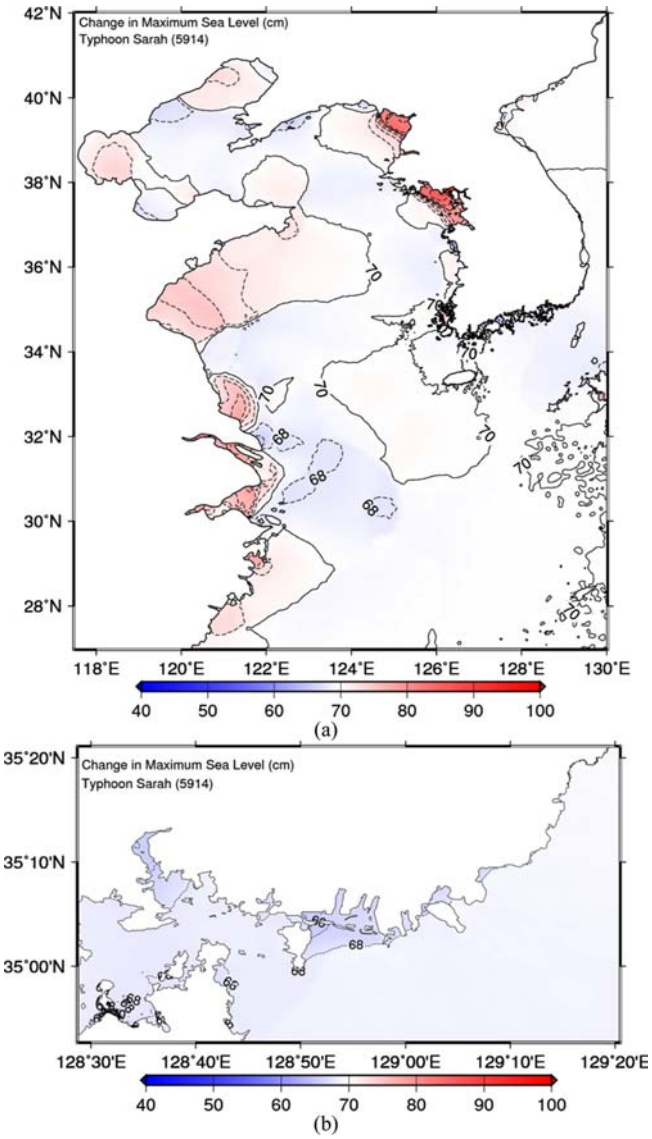

Fig. 12. Change in maximum sea level relative to the land for the 1959 event (Typhoon Sarah) occurring in the year 2100

Here, we estimated the potential change in the water level associated with the MSL rise, i.e. climate change with a 70 cm rise increased the water depth, based on the literature. However, the prediction of changes due to a category 5 equivalent super typhoon requires further refinement and improvement of the climate models (Wolf and Flather 2005).

7. Conclusions

In this study, the integrally coupled tide-surge-wave model (ADCIRC-SWAN) based on an unstructured grid was used to simulate the storm surge and wave caused by Typhoon Sarah (5914) in the Yellow and East China Seas. The model validation was performed by comparing the simulation with some of the available measured water elevation data and previous studies, and as a result, the model systems reproduced reasonable wave and surge properties. To provide useful information for the development of countermeasures against coastal disasters, we calculated the maximum wave and storm surge computed from the coupled model for the Yellow and East China Seas, especially the southern coast of Korea, which was severely damaged by this typhoon. A summary follows. Along the southern coast of Korea, the significant wave height ranged from 2 to 7 m, the mean wave period ranged from 4 to 14 sec, and the positive and negative surge heights were 0.3–1 m and 0.1–0.6 m, respectively (negative surge height not shown here). In addition to the coupled tide-surge-wave (TSW) model, the tide-surge (TS) model and individual tide (T) and wave (W) models were performed to examine the interactions in wave, tide and storm surge processes. In general, for the significant wave height, the independent wave model had a tendency to overestimate compared with the coupled tide-surge-wave model. Similarly, the tide-surge model without coupling the wave overestimated the storm surge. The wave effect was remarkable near the coastal regions, raising the water into these regions. Accordingly, the water elevation increased onshore, and vice versa offshore.

The possible water level change was estimated assuming the recurrence of Typhoon Sarah for a sea level rise of 70 cm, corresponding to the MSL increment in 2100 compared to that of 1980–1999. The change in the maximum sea level

ranged from 80 to 100 cm along the western coast of Korea, e.g. Gyeonggi and Seohan Bays. The range was 70–80 cm along the eastern coast of China. Along the southern coast of Korea, the range was approximately 68 cm. The coupled model used in this study is believed to be an appropriate tool for hindcasting and predicting the tide-surge-wave in the Yellow and East China Seas. Further improvements such as expanding to a three-dimensional tide-surge model will be needed with refinements of the mesh and water depth for the regions of interest.

Acknowledgements

This study was supported by the China-Korea cooperative research project for nuclear safety funded by CKJORC and a major project titled "A Study on the Dispersion of Radioactive Materials and Their Influence on Marine Biota Following the Accidental Release to the Ocean" funded by KIOST. This study was supported by a project of KISTI for the development of an HPC-based management system against a national-scale disaster.

References

Atkinson JH, Westerink JJ, Hervouet JM (2004) Similarities between the wave equation and the quasi-bubble solutions to the shallow water equations. Int J Numer Meth Fl **45**:689–714

Battjes JA (1972) Radiation stresses in short-crested waves. J Mar Res **30**(1):56–64

Booij N, Ris RC, Holthuijsen LH (1999) A third-generation wave model for coastal regions, Part I, Model description and validation. J Geophys Res **104**:7649–7666

Cardone VJ (1969) Specification of the wind distribution in the marine boundary layer for wave forecasting. New York University, New York, Geophysical Sciences Laboratory report TR-69-1, 131 p

Choi BH, Eum HM, Woo SB (2003) Modeling of coupled tide-wave-surge process in the Yellow Sea. Ocean Eng **30**:739–759

Choi BH, Min BI, Kim KO, Yuk JH (2013) Wave-tide-surge coupled simulation for typhoon Maemi. China Ocean Eng **27**(2):141–158

Dawson C, Westerink JJ, Feyen JC, Pothina D (2006) Continuous, discontinuous and coupled discontinuous continuous Galerkin finite element methods for the shallow water equations. Int J Numer Meth Fl **52**:63–88

Dietrich JC, Bunya S, Westerink JJ, Ebersole BA, Smith JM, Atkinson JH, Jensen R, Resio DT, Luettich RA, Dawson C, Cardone VJ, Cox AT, Powell MD, Westerink HJ, Roberts HJ (2010) A high-resolution coupled riverine flow, tide, wind, wind wave and storm surge model for southern Louisiana and Mississippi, Part II: Synoptic description and analyses of Hurricanes Katrina and Rita. Mon Weather Rev **138**:378–404

Fujita T (1952) Pressure distribution within typhoon. Geophys Mag **23**:437–451

Garrat JR (1977) Review of the drag coefficients over oceans and continents. Mon Weather Rev **105**:915–929

Heaps NS (1965) Storm surges on a continental shelf. Philos T R Soc S-A **257**:351–383

Holthuijsen LH, Herman A, Booij N (2003) Phase-decoupled refraction - diffraction for spectral wave models. Coast Eng **49**(4):291–305

Kim KO, Yamashita T (2008) Storm surge simulation using wind-wave-surge coupling model. J Oceanogr **64**:621–630

Kim KO, Yuk JH, Jung KT, Choi BH (2013) Simulation of typhoon Bolaven using integrally coupled tide-surge-wave models based on unstructured grid system. In: Proceedings of the Korean Association of Ocean Science and Technology Societies, Jeju, 23–24 May 2013, pp 1646–1649

Longuet-Higgins MS, Stewart RW (1964) Radiation stresses in water waves; a physical discussions, with applications. Deep Sea Res Oceanogr Abstr **11**(4):529–562

Luettich RA, Westerink JJ (2004) Formulation and numerical implementation of the 2D/3D ADCIRC finite element model version 44.XX. University of North California, 74 p

Matsumoto K, Takanezawa T, Ooe M (2000) Ocean tide models developed by assimilating TOPEX/POSEIDON altimeter data into hydrodynamical model: a global model and a regional model around Japan. J Oceanogr **56**(5):567–581

Min BI (2011) Modeling wind waves and storm surge using intergrally-coupled model. Ph.D. Thesis, Sungkyunkwan University, 174 p

KMA (2014) Report on assessment of climate change in Korea – The scientific evidence of climate change. Korea Meteorological Administration, 305 p (in Korean)

Ozer J, Padilla-Hernández R, Monbaliu Fanjul, EA, Albiach JCC, Osuna P, Yu JCS, Wolf J (2000) A coupling module for tides, surges and waves. Coast Eng **41**:95–124

WAMDI Group (1988) The WAM model—a third generation ocean wave prediction model. J Phys Oceanogr **18**:1775–1810

Westerink JJ, Luettich RA, Feyen JC, Atkinson JH, Dawson C, Roberts HJ, Powell MD, Dunion JP, Kubatko EJ, Pourtaheri H (2008) A basin to channel scale unstructured grid hurricane storm surge model applied to southern Louisiana. Mon Weather Rev **136**(3):833−864

Wolf J, Flather RA (2005) Modelling waves and surges during the 1953 storm. Philos T R Soc A **363**:1359–1375

Zijlema M (2010) Computation of wind-wave spectra in coastal waters with SWAN on unstructured grids. Coast Eng **57**(3):267–277